Relativistic Broadening of the Iron Emission Line from Serpens X-1

Robert Morgan*

Advisor: Edward Cackett†

Abstract

It has been shown that the neutron star and low-mass x-ray binary (LMXB), Serpens X-1, exhibits evidence of a broadened Fe Kα emission line. In this paper, the most recent and longest-to-date *Suzaku* observation of Serpens X-1 is analyzed to test the origin of the Fe Kα line in neutron star LMXBs. Analysis and spectral fitting of this new data with a relativistic emission line model and a blurred disk reflection model seem to agree with previous observations of Serpens X-1 and support constraints placed on the radius of the neutron star, as well as the presence of relativistic effects in the shaping of the iron emission line.

Introduction

In a binary system, it is possible for one of the objects to strip the matter from the other if the former is sufficiently dense. The accreting matter, then, is pulled into a disk around the compact object due to the fact that angular momentum must be conserved. The strong gravity of the compact object accelerates the matter in the disk to relativistic speeds, which can potentially affect observations through doppler and gravitational redshifts.

The process of emission from accretion disks involves a source of hard x-rays being incident on a disk. The x-rays then reflect off of the disk, and can be studied based on the observed emission spectra (Gierliński, M. et al. 1999 [6]; Markoff et. al 2005 [7]; Markoff & Nowak, M. A. 2004 [8]). Due to the combination of the fluorescence and the abundance of iron in the disk, the iron emission line is one of the easiest spectral features to observe (Cackett, E. M. et al. 2010 [3]). By observing and modeling the shape of the iron emission line, it becomes possible to understand the extent of the relativistic effects–which in this case manifest in the red-skewing of the iron line.

In the past, the Fe Kα emission line has been studied by astrophysicists as a means of setting constraints on the equations of state of different varieties of ultra-dense matter (Bhattacharyya, S. & Strohmayer, T. E. 2007 [2]; Cackett et al. 2010 [3]; Miller, J. M. 2007 [10]). By fitting the emission spectrum of a source, it becomes possible to draw conclusions about characteristics and properties of the astronomical body being studied. With the iron line, researchers have been able to approximate the inner radii of accretion disks around neutron stars and black holes (See Cackett et al. 2010 [3] for an analysis of many LMXBs).

In the case of neutron stars, the inner radius of the disk is of particular interest as it allows one to determine the maximum possible radius of the star itself, since the stellar surface cannot extend into the disk, and thus move one step closer to quantifying its equation of state (Bhattacharyya, S. & Strohmayer, T. E. 2007 [2]). Setting constraints on the radii of neutron stars is also useful in understanding the geometry of a potential boundary layer between the disk and the star.

Current research in the field uses the shape of the iron line to probe the dense material that comprises neutron stars. Using models that explain the line shape with effects caused by relativity, it is possible to put constraints on the radii of neutron stars (Cackett, E. M. et al. 2010 [3]).

In this paper, a simple Gaussian component, a component for a relativistic emission line from an accretion disk, and a blurred reflection component (Ballantyne, D. R. 2004 [1]) are all tested in addition to the best-fitting continuum model. The purpose of this paper, then, is to test previously successful models on a new

*Department of Physics and Astronomy, Wayne State University, Detroit, MI 48202, robertmorgan@wayne.edu

†Department of Physics and Astronomy, Wayne State University, Detroit, MI 48202, ecackett@wayne.edu

observation of Serpens X-1 as a method of understanding the origin of the iron line as well as setting constraints on the maximum possible radius of this neutron star.

Before going further, it should be mentioned here that Serpens X-1 is a fairly bright source, so the chances of the effects of pile-up[1] being present in the event files are high. Pile-up can change the shape of the spectrum if enough low-energy photons are misread as high-energy photons, so it becomes important to account for pile-up and to attempt to reduce the effects of it in the data.

The effects of pile-up have been mitigated differently between past observations of LMXBs. For example, the effects of severe pile-up on a spectrum's shape has been studied using *XMM-Newton* by comparing single and double timing mode events, and extracting spectra from different spatial regions (Ng, C. et al. 2010 [11]). However, and more applicably to this paper, circular exclusion regions centered on a source have been used to prevent pile-up from influencing the spectra for *Suzaku* observations (Miller, J. M. et al. 2010 [9]). This paper uses the exclusion region technique with a slight adaption that is discussed in section 2.2.1.

1 Data Collection

The data for this observation of Serpens X-1 were collected by *Suzaku* on three different occasions. For soft x-ray events, data from the three operating x-ray imaging spectrometers (XIS0, XIS1, and XIS3) were studied. Overall, the XIS detectors are most sensitive to energies within the range 1.0-10.0 keV; however, the back-illuminated XIS1 is relatively more sensitive to lower-energy photons than the front-illuminated XIS0 and XIS3. For the harder x-ray events, the PIN-silicon diodes of the hard x-ray detector (HXD/PIN) were used. This detector greatly increases the range of sensitive energies of the telescope beyond 10.0 keV, but for this object and this observation, the spectrum was only fit for 15.0-26.0 keV.

Table 1 includes information on the dates and lengths of each of the periods that were compiled during this observation. For all three periods, XIS0 and XIS1 were operated in the 1/4-window mode, and XIS3 was operated in full-window mode. The burst option was used for all observations, with a 0.1 second burst for the full-window mode and a 0.135 second burst for the 1/4-window mode.

Observation ID	Start Date (DD/MM/YYYY)	Exposure Time (ks)
408033010	01/10/2013	130.329
408033020	13/03/2014	82.358
408033030	10/04/2014	23.027

Table 1: Dates and lengths of each observation period. Exposure times from HXD/PIN detector are listed since the XIS detectors were operated in burst mode.

By expanding the length of the total observation period, these data become comparable in exposure time to previous observations, and modeling the data becomes a reliable method of checking the results of previous attempts of fitting the iron emission line from Serpens X-1.

For this observation, the data from the XIS detectors was taken strictly in burst mode to limit the exposure time per frame and to reduce the effects of pile-up. The window mode mentioned earlier is important to consider because in full-window mode, a readout streak[2] is observable in the event files and can be used to estimate its effects on the 1/4-window mode observations. Both the effects of pile-up and the presence of the readout streak were taken into consideration, and those processes are discussed sections 2.2.1 and 2.2.2 respectively. Also, both 3x3 and 5x5 viewing modes were used in obtaining the data, which meant that another tool was needed to combine the viewing modes; this process is described in sections 2.1 and 2.2.

2 Data Reduction

The standard procedure in the *Suzaku Data Reduction Guide* (also referred to as the *ABC Guide*) was followed when preparing the unfiltered event files for spectral fitting. The processes for the HXD/PIN data and the XIS data are discussed below.

2.1 HXD/PIN Data Reduction

Starting with the HXD/PIN data, the tool `aepipeline` was applied to reprocess, calibrate, and screen the data. When the PIN event files are targeted with `aepipeline`, the tools `hxdgtigen`, `hxdtime`, `hxdpi`, and `hxdgrade` are utilized. More details on

[1] Pile-up is when two (or more) photons from the source strike nearby areas on the detector within a small enough time frame such that they are interpreted by the detector as one photon of higher energy.

[2] A readout streak can occur in full-window mode because as the events are being readout across the detector, incident photons can still be detected.

the individual roles of these tools can be found in the *ABC Guide*. Effects of pile-up on the HXD/PIN detector do not need to be considered because the PIN detector records events using silicon diodes and photomultiplier tubes as opposed to a CCD.

To extract the spectra from each of the observations, the `hxdpinxbpi` tool was utilized. The full function of this tool can be found in the *ABC Guide*, but its main feature is that it produces a spectrum for the source as well as a spectrum that is a combination of the non-x-ray background and the cosmic-x-ray background. By analyzing the total background spectra, it was determined that the background overtook the source spectra after approximately 26.0 keV, and it was for this reason that the spectra for the HXD/PIN detector were only fit over the range 15.0-26.0 keV. Finally, using the `addascaspec` tool, the source spectra for the three observations were combined, and the total background spectra for the three observations were also combined to produce one source spectrum and one background spectrum for the HXD/PIN detector.

2.2 XIS Data Reduction

For the data collected by the XIS detectors, again the first step was to reprocess the data using the tool `aepipeline`, which calibrated the data by applying the following tools in order: `xistime`, `xiscoord`, `xisputpixelquality`, `xispi`, `xisgtigen`, and `xisucode`. The functions of these tools can be found in the *ABC Guide*. An important part of this step in the data reduction process is that events where the telemetry is saturated are filtered out. As Serpens X-1 is a fairly bright source, it was found that a few of the event files showed that the telemetry was saturated. Those times were filtered out in the screening process and did not affect the data when it came to the spectral fitting.

The next step was to use the script `xisrepro` in `xselect`, which makes cuts, filters, and creates cleaned event files from the reprocessed and calibrated event files based on the instructions provided in the *ABC Guide*. The main feature of the script is that it runs the tool `cleansis`, which removes bright and flickering pixels from the data.

As a check to ensure that the data reduction for the XIS data was done correctly, the exposure times of the files that were cleaned manually were compared to the exposure times of the cleaned event files that were provided with the data. In each case it was found that the exposure times were able to be matched between corresponding files–showing that the correct instances were filtered out by the calibration and screening.

2.2.1 Accounting for Pile-up

The influence of pile-up was measured in two ways. First, `SAOImage DS9` was used to draw the largest possible circular inclusion region in the 1/4-window mode (radius=135 pixels), as well as a circular exclusion region of varying radius that was centered on the source–since it was assumed that the effects of pile-up would be most pronounced in the center[3]. The spectra for these regions were then extracted and fit using `diskline` for simplicity. By increasing the radius of the exclusion region and comparing the parameters in each case, it became clear that the parameters of the model we chose began to settle after a radius of 20-30 pixels was used for the exclusion region, and the extracted spectra began to look the same. This result was expected as it agrees with past observations (Cackett et al. 2010 [3]).

The second method of pile-up correction was performed using the tool `ISIS`, which is the *Interactive Spectral Interpretation System*, and a script written for estimating pile-up (Nowak, M. 2010 [12]). The estimate gave a visual representation of which areas were the most piled-up in the cleaned event files.[4] Based on the shapes of the areas with a high pile-up fraction (≥ 0.05), it was found that the areas affected by pile-up were not circularly-distributed about the center of the source, but rather in the shape of a Maltese cross, since this is the shape of the point spread function (PSF) for the telescope. This identification prompted the use of two different types of exclusion regions: a plus-sign-shaped region where each side of the polygon was 30 pixels in length and all angles were right angles; and a four-pointed-star-shaped region where an 18 pixel by 18 pixel box was centered on the source, and then from each corner a line was drawn to points that were 36 pixels directly horizontally or vertically from the center of the box. To make the regions easier to visualize, pictures are displayed in Figure 1.

These exclusion regions seem to be complicated, however, the choice to use them was based on their ability to eliminate piled-up areas while keeping as many data counts as possible. The plus-sign was used on the XIS0 and XIS3 data, while the star was used on

[3]This assumption is based on the fact that pile-up is proportional to the square of the flux, so the brightest areas would naturally be the most piled-up (Yamada, S., et al. 2012 [14])

[4]Nowak's script is not to be used for an exact determination of the pile-up fraction, as it only provides an estimate, but using it as a guide to find which regions show the most severe effects of pile-up is certainly reasonable.

Figure 1: Filtering Regions

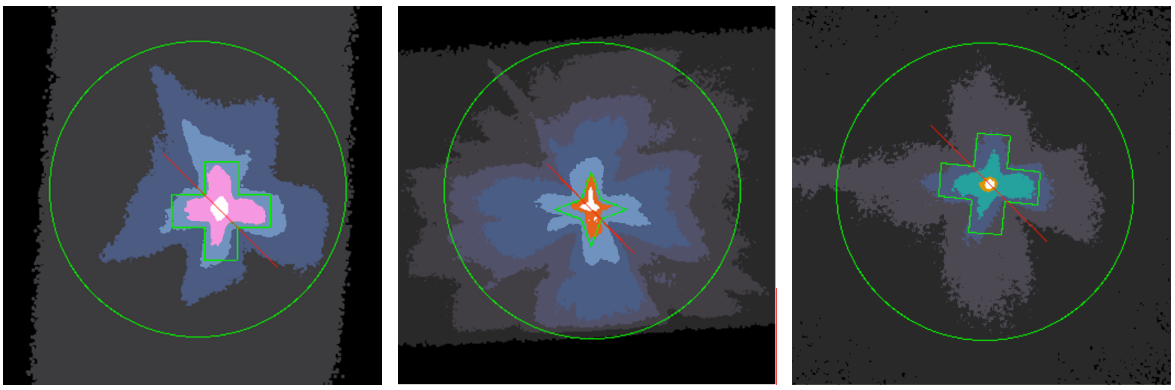

(a) XIS0 (b) XIS1 (c) XIS3

the XIS1 data. It was decided not to use a plus-sign-shaped exclusion region on all three detectors because the models fit slightly better when the star was used for the XIS1 data. In all cases, a circular inclusion region of radius 135 pixels was used, and the exclusion region was placed and rotated in a manner that would eliminate the areas of highest estimated pile-up fraction according to the estimate determined in `ISIS`.

A previous finding in removing the effects of pile-up that should be noted here is that while removing piled-up regions changes the shape of the continuum, the iron line remains remarkably robust (Cackett, E. M., et al. 2010 [3]). This result was determined by excluding circular regions of radii 30 pixels, 60 pixels, and 90 pixels, and then observing the parameters of the model component `diskline`. While the continuum parameters changed slightly with each exclusion region, the line parameters did not change a significant amount. This finding is important to this paper as it implies that extraction regions of any size can be removed without affecting the iron line; thus, it is then possible to remove the effects of pile-up with extraction regions as a means to model the continuum correctly and then proceed to model the iron line.

2.2.2 Accounting for the Readout Streak

The readout streak was present in the data from XIS3, and an example of the streak can be seen in Figure 1c. To account for the readout streak, it was necessary to find the fraction of counts in the inclusion region that were caused by the readout streak, but not removed by the exclusion region. By obtaining the number of data counts taken from a region away from the source but on the readout streak, it was possible to scale the counts to reflect the area of the region, and in that way understand how many counts near the source were the result of the readout streak.

With this process, it was determined that the fraction of events in the source region that were due to the readout streak was on average 0.121 for the full-window mode observations, and this fraction was factored out when it came to fitting the spectra. Using this result, the fraction of events due to a readout streak on the 1/4-window mode observations was inferred to be on average 0.090 based on the difference in exposure times per frame between the full and 1/4-window modes, and the burst settings that were used for those modes.

Once the data had been reprocessed, calibrated, and screened, and after the effects of pile-up and the readout streak had been considered and removed, different models could then be used to fit the data. The process of spectral fitting involves extracting the spectra of all the cleaned event files, combining the spectra, and then fitting the data with different models. To extract the spectra from the regions that were created in `ISIS`, `xselect` was used to filter the cleaned event files and then extract the spectra. In this step, the event files were also checked for the presence of x-ray bursts by examining the light curves, and no x-ray bursts were found. After the spectra were extracted, the next step was to combine the 3x3 and 5x5 viewing modes using the `addascaspec` tool, which yielded one spectrum for each XIS detector that could then be analyzed.

3 Spectral Fitting

The three XIS spectra and the HXD/PIN spectrum, as well as its background spectrum, were loaded into `xspec` and fit over the range 1.0-10.0, 15.0-26.0 keV using multiple models. The energies between 1.45-2.5 keV were consistently ignored due to the appearance of large residuals of what is believed to be instrumental nature (Cackett, E. M., et al. 2010 [3]).[5] First, the energies in the interval 5.0-7.5 keV were ignored so that the continuum could be fit without the iron line. Then, the iron line was taken into consideration and three model components were tested for the best fit: a simple gaussian line profile, `diskline`, and a blurred reflection model. For all models, the fit statistic χ^2 was used to quantify the goodness of the fit.

For the reason of checking and repeating past results, it should be mentioned that a broadened iron emission line was observed for the spectra and is displayed below.

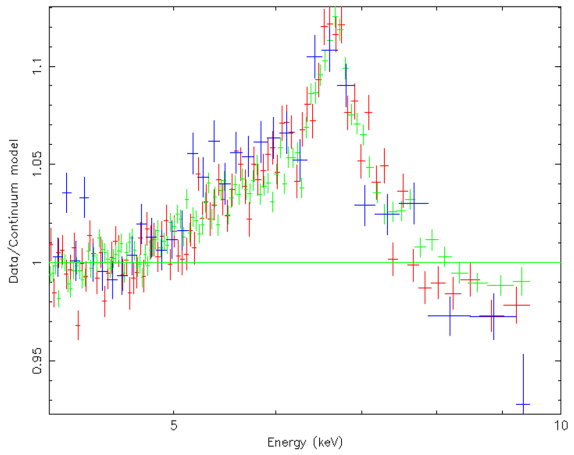

Figure 2: Broadened iron line. Plot obtained from the data/continuum model ratio for energies 4.0-10.0 keV. XIS0 is red, XIS1 is green, and XIS3 is blue.

Clearly, the presence of a broadened iron emission line has again been observed. The remainder of this article will apply different models to the data. The purpose is to determine the best-fitting model for the data, and then to place a constraint on the radius of Serpens X-1.

3.1 Continuum Model

The decision of which models to use was based on which models have been used successfully for past observations (Cackett, E. M., et al. 2008 [4]), and whether or not they improved the fit in a statistically significant way. For the four spectra, it was found that a model with an absorbed disk blackbody component (`diskbb`), plus a single-temperature blackbody component (`bbody`), plus a power law component (`powerlaw`) for the harder states fit the continuum well, as it has in the past observations of LMXBs.

When fitting the continuum, and all other models, several decisions were made for the purpose of a better fit. The first decision was to freeze the constant for the XIS0 spectrum at 1.000, for the reason of scaling the flux in relation to the XIS spectra. The other decision that was made was to untie the normalization parameters of the blackbody components for the XIS1 and XIS3 spectra. The only influence this change had was a slightly lower χ^2 value.

It also should be noted that in the continuum model, as well as in all the other models, the constant for the XIS3 spectrum is much higher than expected, even after accounting for the fraction of counts that were caused by the readout streak. While it is unusual for the constant to be much greater than 1.000, it was necessary in this case for the models to fit the data. The best-fitting model parameters are displayed in Table 2, and are similar to previous fittings (Cackett, E. M. 2008 [4]). The components used in the continuum model and the broadband spectrum are shown in Figure 3. For all broadband spectrum figures, only data from XIS1 is shown because it had the lowest signal-to-noise ratio.

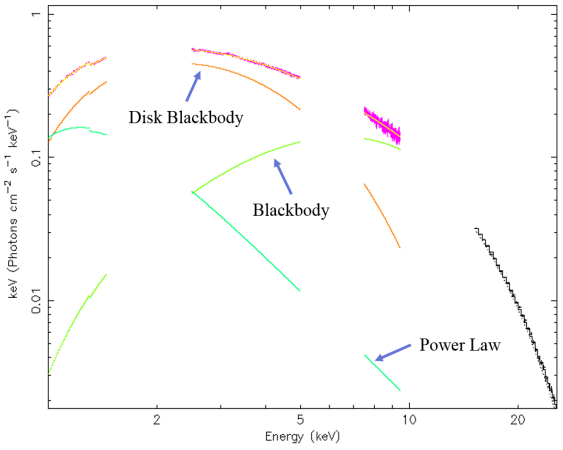

Figure 3: Continuum model components. Only XIS1 and HXD/PIN spectra are shown. This figure allows one to observe the individual components involved in the continuum model.

[5] Cackett, E. M. et al. 2010 ignores the energies 1.5-2.5 keV, however, for this observation it was found that the lower bound needed to be decreased slightly to eliminate the presence of the large residuals.

Model Component	Parameter	Units	HXD/PIN	XIS0	XIS1	XIS3
Constant	Factor	—	0.93 ± 0.03	1.000	1.100 ± 0.002	1.688 ± 0.006
Absorption	N_H (10^{22})	(cm^{-2})	0.58 ± 0.03	—	—	—
Disk Blackbody	T_{in}	(keV)	1.35 ± 0.009	—	—	—
Disk Blackbody	Norm.	—	55 ± 2	—	—	—
Blackbody	kT	(keV)	2.26 ± 0.03	—	—	—
Blackbody	Norm. (10^{-2})	—	2.60 ± 0.03	—	2.52 ± 0.02	2.39 ± 0.04
Power-law	Γ	—	3.2 ± 0.2	—	—	—
Power-law	Norm.	—	0.51 ± 0.08	—	—	—

Table 2: Parameters for the continuum model. $\chi^2/\mathrm{dof} = 1.895$ for 2233 degrees of freedom. A blank value for any of the XIS parameters indicates that it is tied, and hence equivalent, to the parameter for the HXD/PIN spectrum. All uncertainties are 1σ. If there is no uncertainty given, the parameter was frozen.

3.2 Phenomenological Models

Next, the iron line was included in the model. Two additive model components were tested to determine which gave the best fit. The models tested included a simple Gaussian distribution (`gaussian`) and a component for a relativistic accretion disk line emission from a zero-spin black hole (`diskline`).

The first phenomenological model that was tested was a simple Gaussian line profile. This component fit the spectra using parameters for the line energy, the standard deviation, and normalization. The purpose of fitting with a Gaussian distribution is to evidence the observation of a red-skewed iron line. If the Gaussian fits well, it is an indication of a symmetrical iron line; however, when the Gaussian does not fit well, a quantitative understanding of the presence of a skewed emission line can be gained. The parameters for the Gaussian model are displayed in Table 3 and the model components are displayed in Figure 4.

The model component `diskline` involves parameters that fit the spectra based on the line energy, the emissivity index, the inner radius of the disk, the outer radius of the disk (which is frozen at 1000 GM/c^2 by convention), the inclination of the disk, and a normalization parameter. In Cackett, E. M., et al. 2008 [4] and this article, all the `diskline` parameters are allowed to be free with the exception of the outer radius parameter.

`Diskline` is traditionally a model component used for zero-spin black holes. To check its applicability to neutron stars–specifically Serpens X-1–the `laor` model component was also analyzed. The `laor` component is for maximally-spinning black holes and applies when the space is described by the Kerr metric. It was found that the `laor` component led to an inner radius

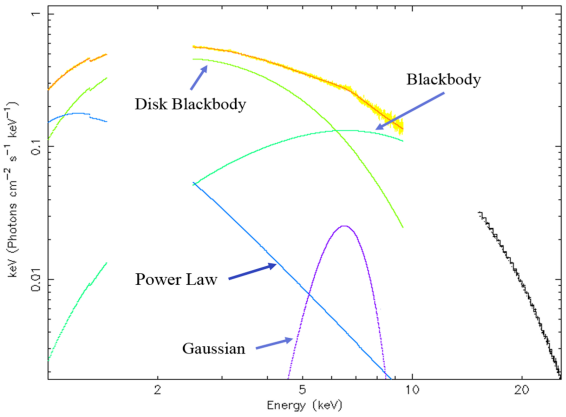

Figure 4: Gaussian model components. Only XIS1 and HXD/PIN spectra are shown. This figure allows one to visually appreciate the addition of the `gaussian` component to the continuum model.

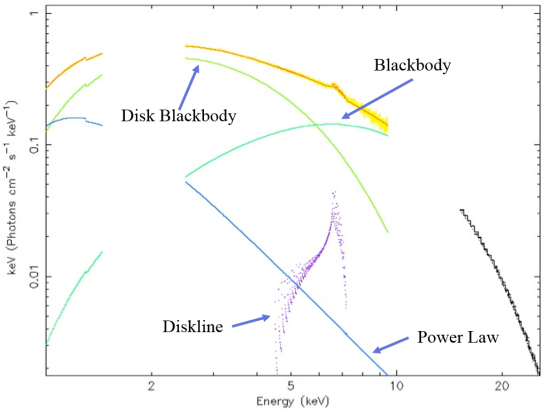

Figure 5: Diskline model components. Only XIS1 and HXD/PIN spectra are shown. Note that the `diskline` component accounts for an asymmetric distribution.

of $7.1^{+0.3}_{-0.1}$ GM/c^2. Since this value is greater than 6 GM/c^2, it is reasonable to assume that the space can be described with the Schwarzschild metric, and there-

fore that the `diskline` component can accurately be applied.

Because `diskline` is intended to model relativistic effects, if it fits the data well there is a good indication that relativity plays a role in broadening the iron line through gravitational and doppler redshifts. The best-fitting parameters for this model are presented in Table 4, and the broadband spectrum can be observed in Figure 5.

3.3 Reflection Models

After fitting the continuum and the iron line with phenomenological models, the next step was to try a more physically-motivated model. The model chosen, because of its success in past observations, was a reflection model of a blackbody from a constant-density, ionized accretion disk (`bbrefl`) (Ballantyne 2004 [1]). To adapt this table model for the relativistic effects of the fast-moving matter in the accretion disk, a convolution model (`rdblur`) was applied. By blurring the emission line model, the component can account for a broadened red wing in addition to normal disk reflection from a blackbody.

The parameters of this model include the log of the ionization parameter, the temperature of the incident blackbody (which is tied to the blackbody temperature parameter in the continuum model in Cackett, E. M., et al. 2010 [3] as well as in this work), the fraction or strength of the reflection off the disk, the redshift, and

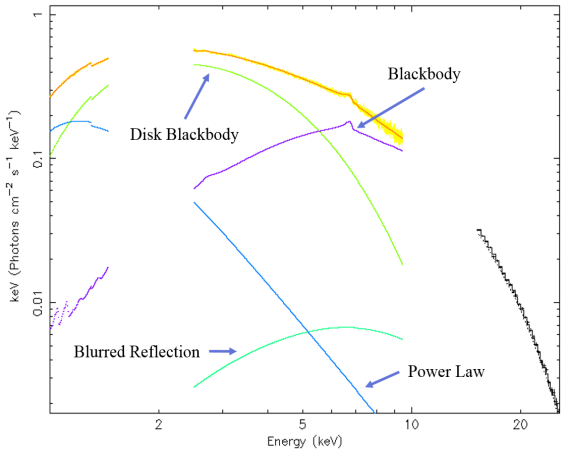

Figure 6: Blurred reflection model components. Only XIS1 and HXD/PIN spectra are shown. Note the addition of the reflection component that was blurred to account for the asymmetric distribution.

a normalization parameter. The convolution model itself has parameters that model the emissivity index, the inner radius of the disk, the outer radius of the disk, and the inclination of the disk. For this component of the model, the outer radius and redshift parameters are frozen while all others were allowed to be free. Table 5 shows the best-fitting parameters for the blurred reflection model, and Figure 6 displays the broadband spectrum.

3.4 Quality of Spectral Fits

Overall, large χ^2 values were obtained for the number of degrees of freedom in the data. While unusual, the higher-than-expected fit statistic was consistent throughout the data. As an attempt to understand the source of the large values, the data/model ratio was examined for each model to search for residuals. The largest residual in the plot was near 3.1 keV, and could have possibly been the emission line of argon (Di Salvo, T. et al. 2015 [5]). However, it was also observed that there was a change in the effective areas of all three XIS detectors near that energy. Upon comparing the percent deviation of the data from the model at 3.1 keV with the average percent decrease in effective area at 3.1 keV, it was determined that the change in area was the most probable cause of the observed residual. The plots can be observed in Figures 7 and 8.

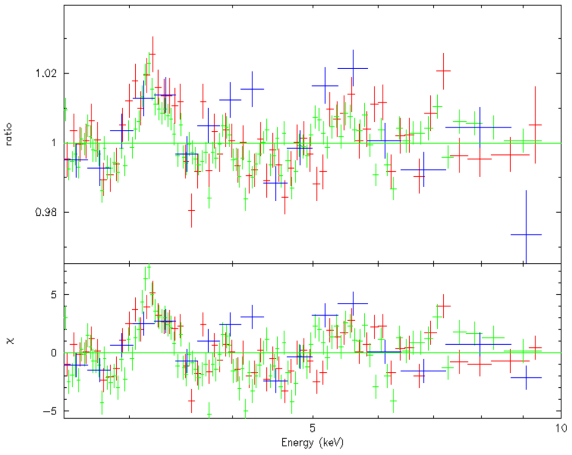

Figure 7: Observed residuals in the data. The plot shows the strongest residual in the data after the iron line was fit. XIS0 is red, XIS1 is green, and XIS3 is blue; the reflection model was used for this plot.

All other residuals in the data/model plot were fit with `diskline` and `gaussian` components to determine if the fit could be improved. In all cases, the chi-squared value did not significantly improve, evidencing that the residuals were not emission lines of other elements in the disk. It was also observed that all the residuals were on the scale of 1%-2% deviation from the models, which means that the most probable cause

Model Component	Parameter	Units	HXD/PIN	XIS0	XIS1	XIS3
Constant	Factor	—	0.91 ± 0.02	1.000	1.099 ± 0.002	1.690 ± 0.005
Absorption	N_H (10^{22})	(cm^{-2})	0.65 ± 0.03	—	—	—
Disk Blackbody	T_{in}	(keV)	1.355 ± 0.009	—	—	—
Disk Blackbody	Norm.	—	57 ± 2	—	—	—
Blackbody	kT	(keV)	2.30 ± 0.01	—	—	—
Blackbody	Norm. (10^{-2})	—	2.58 ± 0.03	—	2.44 ± 0.03	2.32 ± 0.04
Power-law	Γ	—	3.7 ± 0.1	—	—	—
Power-law	Norm.	—	0.71 ± 0.08	—	—	—
Gaussian	Line Energy	(keV)	$6.400^{+0.004}$	—	—	—
Gaussian	Sigma	(keV)	0.83 ± 0.03	—	—	—
Gaussian	Norm. (10^{-3})	—	$7.7 \pm .5$	—	—	—

Table 3: Parameters for the simple gaussian line profile model. $\chi^2/\mathrm{dof} = 1.965$ for 3262 degrees of freedom. A blank value for any of the XIS parameters indicates that it is tied, and hence equivalent, to the parameter for the HXD/PIN spectrum. All uncertainties are 1σ. If there is no uncertainty given, the parameter was frozen.

Model Component	Parameter	Units	HXD/PIN	XIS0	XIS1	XIS3
Constant	Factor	—	0.93 ± 0.03	1.000	1.100 ± 0.002	1.691 ± 0.006
Absorption	N_H (10^{22})	(cm^{-2})	$0.55^{+0.03}_{-0.02}$	—	—	—
Disk Blackbody	T_{in}	(keV)	1.33 ± 0.01	—	—	—
Disk Blackbody	Norm.	—	57 ± 1	—	—	—
Blackbody	kT	(keV)	2.23 ± 0.03	—	—	—
Blackbody	Norm. (10^{-2})	—	2.68 ± 0.03	—	2.55 ± 0.02	2.44 ± 0.03
Power-law	Γ	—	3.1 ± 0.2	—	—	—
Power-law	Norm.	—	$0.45^{+0.04}_{-0.03}$	—	—	—
Diskline	Line Energy	(keV)	$6.9700_{-0.005}$	—	—	—
Diskline	Emissivity Index	—	-4.7 ± 0.2	—	—	—
Diskline	R_{in}	(GM/c^2)	7.9 ± 0.2	—	—	—
Diskline	R_{out}	(GM/c^2)	1000	—	—	—
Diskline	Inclination	(Degrees)	$23.8^{+0.6}_{-0.5}$	—	—	—
Diskline	Norm. (10^{-3})	—	$5.2 \pm .2$	—	—	—

Table 4: Parameters for the relativistic ionized accretion disk emission line model. $\chi^2/\mathrm{dof} = 1.889$ for 3260 degrees of freedom. A blank value for any of the XIS parameters indicates that it is tied, and hence equivalent, to the parameter for the HXD/PIN spectrum. All uncertainties are 1σ. If there is no uncertainty given, the parameter was frozen.

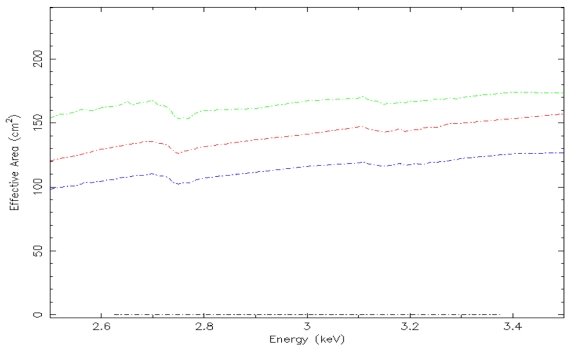

Figure 8: Effective areas of XIS detectors. The plot shows a slight decrease near 3.1 keV for all three detectors. XIS0 is red, XIS1 is green, and XIS3 is blue; the reflection model was used for this plot.

of the residuals was the calibration of the instruments used in the observation. Because the chi-squared value was consistently high, and because that high value can be explained, it will still be utilized to compare the goodness of the fits between the models.

4 Discussion

As in past observations of Serpens X-1 (Bhattacharyya, S. & Strohmayer, T. E. 2007 [2]; Cackett, E. M. et al. 2008 [4]), a broadened red wing of the iron emission line has been observed. This fact was shown visually, as well as through the Gaussian model component, which fit the data the worst of all the models.

Model Component	Parameter	Units	HXD/PIN	XIS0	XIS1	XIS3
Constant	Factor	—	0.86 ± 0.01	1.000	1.099 ± 0.002	1.690 ± 0.005
Absorption	N_H (10^{22})	(cm^{-2})	0.71 ± 0.02	—	—	—
Disk Blackbody	T_{in}	(keV)	1.28 ± 0.01	—	—	—
Disk Blackbody	Norm.	—	71 ± 3	—	—	—
Blackbody	kT	(keV)	2.31 ± 0.02	—	—	—
Blackbody	Norm. (10^{-3})	—	$2.6^{+1.9}_{-0.3}$	—	$1.3^{+1.9}_{-0.2}$	$1.40^{+0.05}_{-0.01}$
Power-law	Γ	—	4.0 ± 0.2	—	—	—
Power-law	Norm.	—	0.9 ± 0.1	—	—	—
Convolution	Emissivity Index	—	-2.40 ± 0.05	—	—	—
Convolution	R_{in}	(GM/c^2)	$6.0^{+0.5}$	—	—	—
Convolution	R_{out}	(GM/c^2)	1000	—	—	—
Convolution	Inclination	(Degrees)	15^{+1}_{-3}	—	—	—
Reflection	$\log \xi$	—	2.37 ± 0.03	—	—	—
Reflection	Fraction	—	0.9 ± 0.1	—	—	—
Reflection	Norm. (10^{-25})	—	1.01 ± 0.08	—	—	—

Table 5: Parameters for the blurred reflection model. $\chi^2/\mathrm{dof} = 1.849$ for 3259 degrees of freedom. A blank value for any of the XIS parameters indicates that it is equivalent to the parameter for the HXD/PIN spectrum. All uncertainties are 1σ. If there is no uncertainty given, the parameter was frozen.

The worse fit of the Gaussian model is evidence of an asymmetric distribution of the iron line. Comparing this quantitative evidence for a skewed emission line with the graph of the data plotted against the continuum model leads to the conclusion that the iron line does in fact display a broadened red wing. Using the other phenomenological model as well as the blurred reflection model, it was then possible to draw conclusions about Serpens X-1 based on the fits of the red-skewed iron line.

The addition of the `diskline` component to the continuum model resulted in an improved fit. The fact the `diskline` component fit the data well evidences the claim that the iron line originates in the inner accretion disk. For the component to fit the data, there must be a relativistic blurring of the iron emission line. Since this blurring was observed, one can draw the conclusion that the line must come from the inner disk, where the relativistic effects would be the strongest and most present in the data.

The physically-motivated reflection model that was used in this paper fit the data best of all the models attempted. Because the reflection model fit well comparatively, it is probable that a blackbody reflecting off the disk is the source of the emission from the disk. This blackbody could potentially be a boundary layer between the accretion disk and Serpens X-1, so further exploration of reflection models could lead to a better understanding of the exact geometries of the boundary layer and the disk itself.

The models in this paper suggest that matter in the disk moving with relativistic velocities as well as the severely-curved spacetime near the neutron star cause the broadening of the red wing, however, other models have been successfully used in the past to explain the red wing without relativistic effects. These models indicate that photons could be downscattered by electrons in a diverging wind across the disk, which could lead to the observed redshift (Titarchuk, L., Laurent, P., & Shaposhnikov, N. 2009 [13]). The diverging wind model, though it may fit the data well, does not seem to be physically accurate. The reasons for this statement include the requirement of a large number of electron scatters in the wind, and the fact that an obscuration of the outer disk from the outflow has not yet been observed (Cackett, E. M. et al. 2010 [3]).

As for the computation of the inner disk radii, from the `diskline` model, the inner radius of the disk can be computed to be 16.3 ± 0.4 km, and from the reflection model it is $12.4^{+1.0}$ km with all uncertainties being 1σ. These calculations were all made assuming a mass of $1.4 M_\odot$. Thus, the inner radius of the disk can be constrained between 12.4 km and 16.7 km, which agrees with previous observations (Cackett, E. M. et al. 2008 [4]). More likely than not, tighter constraints could have been placed on the radius of Serpens X-1 had the instrumental calibration not manifested as an issue in the fits.

Conclusions

This paper confirms two previous findings: a red-skewed iron emission line can be observed in Serpens X-1, and the inner radius of the accretion disk around the star is between 12.4 km and 16.7 km. This constraint on the inner radius leads to a constraint on the maximum possible radius of the neutron star, since the star must be encircled by the disk.

This paper also provides evidence for the applicability of relativistic models to the broadened iron line. It is hoped that tighter constraints can be placed on the inner radius of the disk so that the boundary layer can be fully understood, and so that the equation of state for ultra-dense matter like neutron stars can be quantified.

References

[1] Ballantyne, D. R. 2004, MNRAS, 351, 57

[2] Bhattacharyya, S. & Strohmayer, T. E. 2007, ApJ, 664, L103

[3] Cackett, E. M., et al. 2010, ApJ, 720, 205

[4] Cackett, E. M., et al. 2008, ApJ, 674, 415

[5] Di Salvo, T. et al. 2015, MNRAS, 449, 2794

[6] Gierliński, M. et al. 1999, MNRAS, 309, 496

[7] Markoff et. al 2005, ApJ, 609, 972

[8] Markoff & Nowak, M. A. 2004, ApJ, 635, 1203

[9] Miller, J. M. et al. 2010, ApJ, 724, 1441

[10] Miller, J. M. 2007, ARA&A, 45, 441

[11] Ng, C. et al. 2010, A&A, 522, A96

[12] Nowak, M. 2010, Pile_estimate.sl, retrieved from `http://space.mit.edu/ASC/software/suzaku/pile_estimate.sl`

[13] Titarchuk, L., Laurent, P., & Shaposhnikov, N. 2009 ApJ, 700, 1831

[14] Yamada, S., et al. 2012, PASJ, 64, 53